

Title

Dynamic fluctuations in global brain network topology characterize functional states during rest and behavior

Authors

James M. Shine^{1,2}, Peter T. Bell³, Oluwasanmi Koyejo¹, Patrick G. Bissett¹, Krzysztof J. Gorgolewski¹, Craig A. Moodie¹, and Russell A. Poldrack¹

Affiliations

1 – Department of Psychology, Stanford University, Stanford, CA, USA

2 – Neuroscience Research Australia, The University of New South Wales, Sydney, NSW, Australia

3 – Queensland Brain Institute, The University of Queensland, Brisbane, QLD, Australia

Corresponding author:

James M. Shine – macshine@stanford.edu

Abstract

Higher brain function relies upon the ability to flexibly integrate information across specialized communities of macroscopic brain regions, but it is unclear how this mechanism manifests over time. Here we characterized patterns of time-resolved functional connectivity using resting state and task fMRI data from a large cohort of unrelated subjects. Our results demonstrate that dynamic fluctuations in network structure during the resting state reflect transitions between states of integrated and segregated network topology. These patterns were altered during task performance, demonstrating a higher level of network integration that tracked with the complexity of the task and correlated with effective behavioral performance. Replication analyses demonstrated that the results were reproducible across sessions, sample populations and datasets. Together these results provide insight into the brain's coordination between integration and segregation and highlight key principles underlying the reorganization of the network architecture of the brain during both rest and behavior.

Introduction

A fundamental characteristic of higher brain function is the ability to flexibly integrate communication between a range of specialized sub-networks (1,2). To achieve this dynamic equilibrium, it has been hypothesized that the human brain strikes a metastable balance between the local segregation of function and the global integration of information (3-6). An emerging picture from this recent work suggests that a relatively fixed structural scaffold gives rise to a highly dynamic functional landscape (1,7-9), in which the emergence of momentary neural coalitions forms the basis for complex cognitive functions (10), learning (11) and consciousness (12). Functional neuroimaging studies have confirmed that global brain patterns transition between states of high and low connectivity strength over time (13) and that these fluctuations are related to distinct patterns of network topology (9). Despite these findings, the manner by which these fluctuations in neural organization evolve over time, both during rest and as a function of cognitive states, remains poorly understood.

In this study, we capitalize on recent advancements in high-speed fMRI acquisition by analyzing sub-second resolution resting state and task data using a recently-described metric for time-resolved connectivity analysis (14). Our examination of the evolution of network structure over the course of seconds to minutes demonstrates that the human brain traverses a network state space that fluctuates between topological configurations that emphasize either segregation or integration. We then show that the balance between these states is altered as a function of task complexity and further, that the extent of task-based reconfiguration of network architecture selectively correlates with measures of task performance.

Results

Dynamic Fluctuations in Network Cartography

To characterize time-resolved network topology, we computed region \times region time-resolved functional connectivity matrices using the Multiplication of Temporal Derivatives (MTD) (14) within a sliding temporal window of 10 seconds (*Materials and Methods*; Figure S1) from a cohort of 92 unrelated subjects obtained from the Human Connectome Project (HCP) (15). We then performed community detection within each window, which enabled the estimation of the within- (W_T) and between-module (B_T) connectivity for each region (*Materials and Methods*; Figure 1d) (16-18). While previous studies have successfully partitioned complex biological networks using pre-defined cartographic boundaries (16,19), we hypothesized that the brain should exhibit metastable dynamics, and hence, should fluctuate between cartographic extremes that were characterized by either segregation (i.e. the extent to which the brain is comprised of tight-knit communities of regions) or integration (i.e. the extent to which the modular architecture of the brain is reorganized to allow links between otherwise disparate regions), which might otherwise be obscured by reduction into cartographic classes.

Cartographic Profiling

To test this hypothesis, we created a novel analysis technique to assess the temporal classification into two states without requiring the classification of each node into a pre-defined cartographic class (16). For each temporal window, we computed a joint histogram of within- and between-module connectivity measures, which we refer to here as a “cartographic profile”. K-means clustering of these full profiles across time ($k = 2$, although the results were stable for $k > 2$; see *Materials and Methods*) confirmed the identification of two relatively

integrated and segregated states (Figure 1b/c). The resting brain explored a dynamical repertoire within this topological space, fluctuating aperiodically between the integrated and segregated temporal states (see Figure 1b/c and also Figures S8 & S9 for movies demonstrating the fluctuations of the cartographic profile over time). Importantly, these fluctuations occurred significantly more frequently in the resting data than in a stationary null model. Specifically, $16.1 \pm 1.1\%$ of the window-to-window deviations in mean W_T in the resting state data (mean: 0.025 ± 0.02 W_T bins) exceeded the 95th percentile of the deviations observed in the stationary null model (mean: 0.027 ± 0.01 bins; 95th percentile: 0.051). The two states also showed differential patterns of functional connectivity, with the more integrated state characterized by increased connectivity between default/frontoparietal systems and primary processing networks, such as the auditory, somatosensory and visual networks. In contrast, the segregated state demonstrated stronger within-network connectivity in both the default and frontoparietal systems, however both of these networks became functionally detached from a range of primary processing systems (Figure S5; FDR $q < 0.05$).

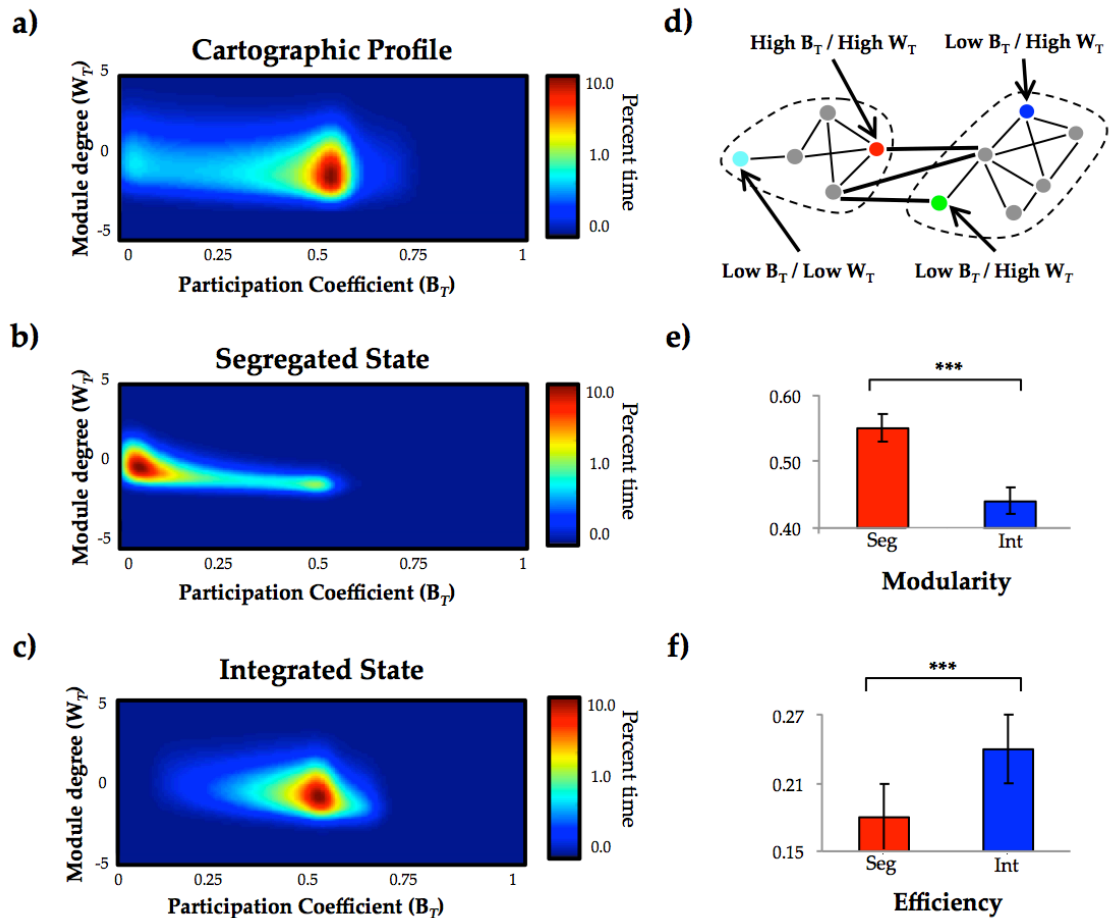


Figure 1: Dynamic Cartographic Analysis. a) The mean cartographic profile joint histogram comparing each region's within- (W_T) and between-module (B_T) connectivity) across all temporal windows in the discovery cohort; b) mean cartographic profile of the Segregated state; c) mean cartographic profile of the Integrated state; d) schematic diagram of the cartographic properties of complex networks; e) temporal windows associated with the segregated state were associated with significantly greater modularity; f) temporal windows associated with the integrated state were associated with increased global efficiency. Key: *** - significant at $p < 0.001$.

Using graph theory, complex network architectures can be summarized using global topological statistics that reflect their underlying organizational structure {Sporns:2013bw}. For instance, the 'modularity' of a network describes the degree to which the connections within a network cohere into tightly connected communities, and as such, can be used as an index of the relative segregation of a

network. In contrast, the global efficiency, which tracks the extent to which two distinct nodes within a network can ‘communicate’ via intermediate regions, can be taken to reflect the extent of integration within a network. Using these two measures, we were able to show that the two temporal states identified using dynamic cartography were associated with distinct topological signatures: as predicted, temporal windows associated with the segregated state had significantly elevated modularity ($Q_s = 0.55 \pm 0.1$ *vs.* $Q_I = 0.42 \pm 0.2$; $p < 0.001$; Figure 1e) whereas those associated with the integrated state had greater global efficiency ($E_s = 0.18 \pm 0.03$ *vs.* $E_I = 0.24 \pm 0.05$; $p < 0.001$; Figure 1f). This topological double dissociation suggests that the dynamic fluctuations in network structure may constrain global information processing, and provide further evidence that the brain fluctuates between states with distinct topologies, and by inference, different modes of information processing (Figure 1e/f).

Task-based Alterations in Cartographic Profile

A direct prediction from our findings from the time-resolved resting analysis was that the balance between network integration and segregation within the brain should track ongoing cognitive function over time. We tested this hypothesis using data from two tasks from the HCP (20) in the discovery cohort of 92 subjects: a simple Motor task and a more cognitively-challenging visual N-back task. We observed a distinct alteration in the cartographic profile during the performance of both tasks when compared to the resting state (Figure 2a/b), suggesting that the brain had entered into a state of higher integration in order to meet the demands of the task. Importantly, performance of the N-back task involved a larger shift towards integration than the Motor task, suggesting that the extent of reconfiguration during task performance varied as a function of the cognitive demands of the task (Figure 2c/d). We quantified this effect by

estimating the affine transformation required to align each subjects' resting cartographic profile with their profile during task. This analysis demonstrated that the N-back task caused a shift towards a more integrated network topology relative to the Motor task (transformation along the B_T axis – N-back: +0.25; Motor: +0.18; $t_{91} = 5.18$, $p < 0.001$; Figure 2c).

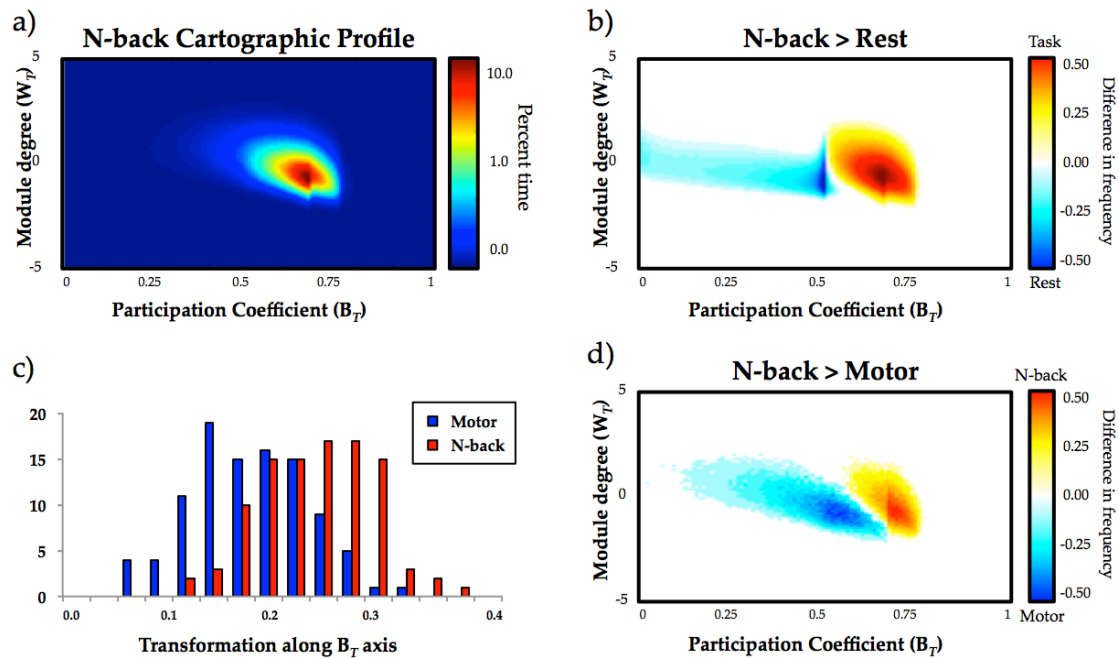


Figure 2: Alteration of cartographic profile during task performance: a) the mean cartographic profile of the N-back task; b) regions of the 2-dimensional joint histogram space that were significantly different between N-back task blocks and the resting state (paired-samples t-test) – colored points indicate a region that survived false discovery correction ($q < 0.05$): yellow/red – increased frequency during N-back task blocks; blue/light blue – increased frequency during resting state; c) histogram reflecting the affine transformation parameter required to match each participants' resting state cartographic profile (along the between-module (B_T) connectivity axis) to the cartographic profile during the each task (Motor – blue; N-back – red); d) significant differences between the cartographic profiles of the N-back and Motor tasks. Key: *** - significant at $p < 0.001$.

Across the cohort of 92 subjects, we observed significant relationships between the cartographic profile and behavioral performance on the N-back task. Specifically, accurate performance on the task was positively correlated with a shift towards integration and inversely correlated with a shift towards segregation (Figure 3a). The mean reaction time on the N-back task also showed a significant relationship with the cartographic profile, such that the extent of integration predicted faster responses across the group (Figure 3b), suggesting that a more integrated state allowed both faster and more accurate responses to the N-back task. There were no performance measures directly associated with the Motor task, which precluded interrogation of behavioral effects in this task. Importantly, neither cartographic profile showed any significant correlations with three measures irrelevant to these tasks (olfaction, audition and positive affect), suggesting that the behavioral relationships with the cartographic profile were specific to task performance. In addition, both tasks showed task-related increases in global efficiency ($r_{Mot.E}: 0.354 \pm 0.03$; $r_{Nback.E}: 0.340 \pm 0.04$) and decreases in modularity ($r_{Mot.Q}: -0.312 \pm 0.02$; $r_{Nback.Q}: -0.333 \pm 0.05$), further implicating the need to flexibly trade-off global topological properties in order to complete the behavioral tasks (21) (see Figure S10 for a movie of the fluctuations as a function of the N-back task). Together, these results suggest that the performance of psychological tasks causes a targeted reorganization of the integrative core of the brain into a unique network assembly that is integral for the performance of each task (22,23).

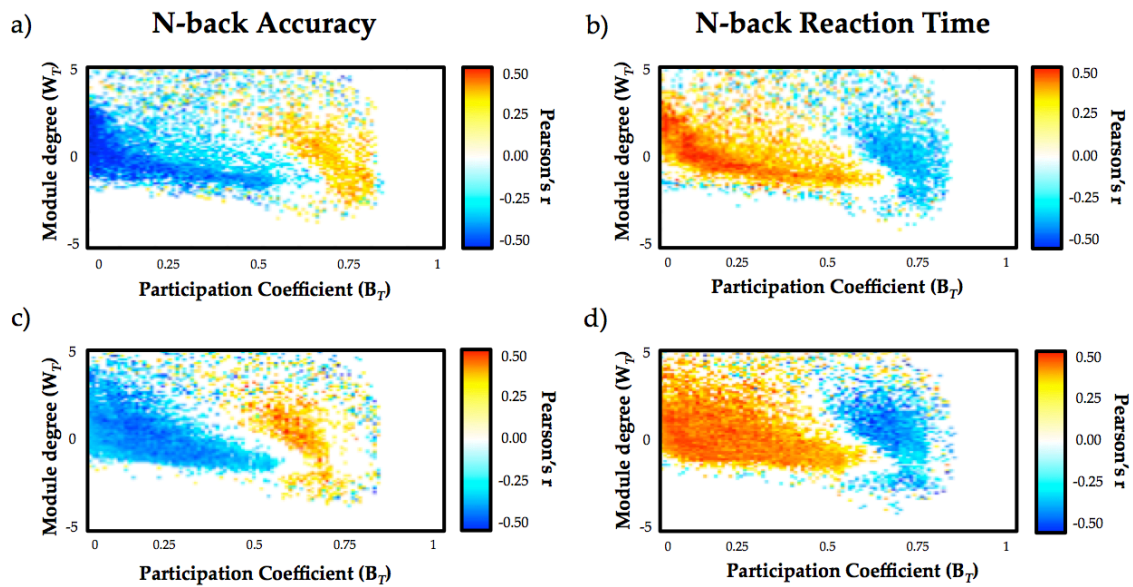


Figure 3 – Relationship between task performance and cartographic profile: a) group-level correlation between accuracy on the N-back task (% trials correct) and each bin of the mean cartographic profile during the N-back task; b) group-level correlation between mean reaction time on the N-back task (msec) and each bin of the mean cartographic profile during the N-back task. Each of these effects was replicated in the second sample of 92 unrelated subjects: c) N-back cartographic profile *vs* accuracy; d) N-back cartographic profile *vs* reaction time. Results represent correlation coefficients that survived multiple comparisons correction (false discovery rate: $\alpha = 0.05$).

Reproducibility

To test the reproducibility of our results, we performed three separate replication analyses: i) on a second resting state session (with identical imaging parameters) from the same cohort of 92 unrelated subjects; ii) on a different cohort of 92 unrelated subjects (with identical imaging parameters) from the HCP consortium; and iii) on 152 subjects from a separate dataset acquired at a different scanning site, acquired using high-resolution functional data from the NKI Rockland dataset (19). In each case, we replicated the analyses described

above on each subject and then summarized each outcome measure of interest at the group level (only resting data were available for the NKI dataset). We then compared the results obtained from the replication with the results obtained from the original sample using a parcel-wise Pearson's correlation coefficient. For each analysis, we observed strong positive correlations between the summary measures derived from each analysis (minimum $r = 0.564$; all $p < 0.001$; see *Materials and Methods*), suggesting that the time-resolved measures identified in this study were reliable across sessions, individuals and even across datasets collected using different scanners and imaging protocols. Each of the relationships identified between the cartographic profile and behavior were replicated in the second set of 92 individuals from the HCP (Both $r > 0.610$; $p < 0.001$; Figures 4c & 4d).

Discussion

In this study, we mapped the spatiotemporal dynamics of complex network structure in the human brain, revealing a dynamical system that fluctuates between segregated and integrated network topology (Figure 1). The cartographic profile of the resting brain was modulated by the performance of both a simple motor and more cognitively-demanding N-back task, both of which caused a targeted reorganization of network architecture into an integrated neuronal assembly that varied as a function of task complexity (Figure 2). Importantly, the extent to which the brain was reconfigured as a function of task was correlated with improved performance accuracy and reaction time on the N-back task (Figure 3), suggesting that the reorganization of the functional connectome into integrated topological states is crucial for the successful engagement of cognitive functions.

Our results demonstrate that the functional neural landscape spontaneously transitions between coordinated assemblies of node classes that comprise one state of high modularity and low global efficiency and another contrasting topological state of reduced modularity and higher global efficiency (Figure 1e/f). These findings suggest that the resting brain consists of a dynamically evolving neural architecture, in which a strongly integrated core inter-connects a range of other regions, with the majority of the brain remaining relatively isolated from the core. As such, our results suggest that the patterns observed in time-averaged analyses of the resting brain may be composed of a combination of different signals – those demonstrating baseline levels of communication between relatively segregated regions that closely mirror the structural connectome (8) and those reflective of the functional activity superimposed onto the idling architecture of the brain, such as the patterns tracking the internal cognitive state over time (24).

This hypothesis is supported directly by our finding that the global information processing state of the brain was altered during the performance of both a simple Motor task, as well as an N-back task that recruits working memory maintenance and updating (Figure 3). Importantly, the extent of reconfiguration of the cartographic profile was related to successful task performance in the N-back task, with the extent of integration correlated with increased response accuracy and decreased response time, suggesting that the cartographic profile is capable of tracking a behaviorally relevant index of neural organization. Interestingly, the extent of integration in the cartographic profile differed as a function of task complexity, suggesting that the completion of the N-back task required more extensive network reorganization than the more simple Motor task, a finding consistent with recent work that demonstrated an increase in modularity (and

hence, segregation) as a function of motor automaticity (11). Although not systematically studied here, it follows that specific departures from the resting spatiotemporal architecture should be observed during the performance of a range of other behavioral tasks (10,25), as well as during sleep and in neurological and psychiatric disease states.

Although the functional implications of our analyses require further confirmation, one potential hypothesis is that the topological fluctuations identified in our study reflect ongoing activity within the so-called 'dynamic core' of the brain (26,27). There is already strong empirical support for these concepts in the neuroscience literature (6), predominantly from global workspace theories of consciousness in which the widespread 'distribution' of information is proposed to mediate conscious experience (2). Indeed, given the known importance of whole-brain integration for the execution of complex behavior (28), the cartographic profile within each window represents an attractive candidate for tracking the activity within the global workspace over time. Thus, these results suggest that it is necessary to move beyond purely structural descriptions of the connectome, and towards detailed knowledge of time-varying spatiotemporal patterns of neural activity that unfold within the structural scaffold of the brain.

Materials and Methods

Data acquisition

For the primary discovery analysis, minimally preprocessed resting fMRI data were acquired from 100 unrelated participants from the Human Connectome Project (mean age 29.5 years, 55% female) (30). For each participant, 14 minutes 30 seconds of resting state data were acquired using multiband gradient-echo echoplanar imaging. The following parameters were used for data acquisition: relaxation time (TR) = 720 ms, echo time = 33.1 ms, multiband factor = 8, flip angle = 52 degrees, field of view = 208x180 mm (matrix = 104 x 90), 2x2x2 isotropic voxels with 72 slices, alternated LR/RL phase encoding.

In addition to the discovery analysis, we also performed an extensive series of replication analyses including: i) data from the same participants using resting state data acquired during a second rest scan during the same scanning session; ii) an independent cohort of 100 unrelated participants from the HCP dataset using identical acquisition parameters at the same scanning site; and iii) an out-of-sample replication using data collected from the NKI Rockland sample (TR = 650msec; voxel-size 3mm³) as part of the 1000 Functional Connectomes Project (31).

Data pre-processing

Bias field correction and motion correction (12 linear DOF using FSL's FLIRT) were applied to the HCP resting state data as part of the minimal preprocessing pipeline (30). The first 100 time points were discarded from the data due to the presence of an evoked auditory signal associated with noise in the scanner. Resting state data acquired from the NKI Rockland sample were realigned to correct for head motion and then each participants' functional scans were

registered to both their T1-weighted structural image and then to the MNI152 atlas using boundary based registration (<http://fsl.fmrib.ox.ac.uk/fsl/fslwiki/>) and Advanced Normalization Tools software (32). After co-registration, data were manually inspected and of the 173 original participants, 11 [6.3%] scans were discarded due insufficient coverage of orbitofrontal cortex, temporopolar cortex and/or cerebellum.

Temporal artifacts were identified in each dataset by calculating framewise displacement (FD) from the derivatives of the six rigid-body realignment parameters estimated during standard volume realignment (33), as well as the root mean square change in BOLD signal from volume to volume (DVARs). Frames associated with $FD > 0.5\text{mm}$ or $DVARs > 5\%$ were identified, and participants with greater than 20% of the resting time points exceeding these values were excluded from further analysis (HCP group 1: 8/100; HCP group 2: 8/100; NKI group: 10/162). Due to concerns associated with the alteration of the temporal structure of the images, the data used in the main analysis were not 'scrubbed' (33), however we did explicitly compare the results of our experiment with scrubbed data (missing values were corrected using interpolation) and found strong correspondence between the outcome measures of the two studies (see *Validation*). Following artifact detection, nuisance covariates associated with the 12 linear head movement parameters (and their temporal derivatives), FD, DVARs, and anatomical masks from the cerebral spinal fluid and deep cerebral white matter were regressed from the data using the CompCor strategy (34). Finally, in keeping with previous time-resolved connectivity experiments (11), a temporal band pass filter ($0.071 < f < 0.125$ Hz) was applied to the data (see *Validation*).

Brain parcellation

Following pre-processing, the mean time series was extracted from 375 pre-defined regions-of-interest (ROI). To ensure whole-brain coverage, we extracted: 333 cortical parcels (161 and 162 regions from the left and right hemispheres, respectively) using the Gordon atlas (35), 14 subcortical regions from Harvard-Oxford subcortical atlas (<http://fsl.fmrib.ox.ac.uk/>), and 28 cerebellar regions from the SUI atlas (36) for each participant in the study.

Multiplication of temporal derivatives

To estimate functional connectivity between the 375 ROIs, we used a recently described statistical technique (Multiplication of Temporal Derivatives; MTD – <http://github.com/macshine/coupling/>) (14) that allows greater temporal resolution of time-resolved connectivity in BOLD time series data when compared to the conventional sliding-window Pearson's correlation coefficient (14). The MTD is computed by calculating the point-wise product of temporal derivative of pairwise time series (Equation 1). In order to reduce the contamination of high-frequency noise in the time-resolved connectivity data, the MTD is averaged by calculating the mean value over a temporal window, w (<https://github.com/macshine/coupling/>).

$$MTD_{ijt} = \frac{1}{w} \sum_t^{t+w} \frac{(dt_{it} \times dt_{jt})}{(\sigma_{dt_i} \times \sigma_{dt_j})} \quad [1]$$

Equation 1 – Multiplication of Temporal Derivatives, where for each time point, t , the MTD for the pairwise interaction between region i and j is defined according to equation 1, where dt is the first temporal derivative of the i^{th} or j^{th} time series at time t , σ is the standard deviation of the temporal derivative time series for region i or j and w is the window length of the simple moving

average. This equation can then be calculated over the course of a time series to obtain an estimate of time-resolved connectivity between pairs of regions.

Time-resolved functional connectivity

Time-resolved functional connectivity was calculated between all 375 brain regions using the MTD (14) within a sliding temporal window of 14 time points (10.1 seconds for HCP; 16 time points for NKI data ~ 10.4 seconds). Previous work has shown that, when using the MTD, a window length of 7 time points provides optimal sensitivity and specificity for detecting dynamic changes in functional connectivity structure in simulated time series data (14). To balance these benefits with the need to track changes in slow cortical fluctuations which are hypothesized to fluctuate at ~0.1 Hz (8), we used a temporal window of 14 time points to calculate a simple moving average of the MTD, which allowed for estimates of signals at approximately 0.1 Hz. Individual functional connectivity matrices were calculated within each temporal window, thus generating an unthresholded (that is, signed and weighted) 3D adjacency matrix (region \times region \times time) for each participant (Figure S1).

Vector autoregressive null model

For each time-resolved outcome measure derived in the above analyses, results were directly compared to data simulated using a series of stationary, multi-dimensional vector autoregressive (VAR) models, which were used to generate surrogate regional time series satisfying the null hypothesis of a linearly correlated, stationary, multivariate stochastic process (Figure S1). In keeping with Zalesky et al. (13), VAR model order was set at 11, appropriately mimicking the expected temporal signature of the BOLD response in 0.72s TR data. The mean covariance matrix across all 92 subjects from the discovery group was used

to generate 2500 independent null data sets, which allows for the appropriate estimation of the tails of non-parametric distributions (37). These time series were then filtered in a similar fashion to the BOLD data. For each analysis, the maximum statistic was concatenated for each independent simulation and then used to populate a null distribution, against which each outcome measure was compared. Null hypotheses were rejected if the observed test statistic was greater than or less than 2.5% of the most extreme values generated by the 2500 VAR trials. Importantly, by comparing each time-resolved outcome measure with the results from the VAR simulations, we could effectively determine whether or not the time-resolved measures allowed for the rejection of the null hypothesis of temporal stationary (Figure S1).

Time- resolved community structure

The Louvain modularity algorithm from the Brain Connectivity Toolbox (BCT; (38) was used in combination with the MTD to estimate both time-averaged and time-resolved community structure. The Louvain algorithm iteratively maximizes the modularity statistic, Q , for different community assignments until the maximum possible score of Q has been obtained (see Equation 2). The modularity estimate for a given network is therefore a quantification of the extent to which the network may be subdivided into communities with stronger within-module than between-module connections.

$$Q_T = \frac{1}{v^+} \sum_{ij} (w_{ij}^+ - e_{ij}^+) \delta_{M_i M_j} - \frac{1}{v^+ + v^-} \sum_{ij} (w_{ij}^- - e_{ij}^-) \delta_{M_i M_j} \quad [2]$$

Equation 2 – Louvain modularity algorithm, where v is the total weight of the network (sum of all negative and positive connections), w_{ij} is the weighted and signed connection between regions i and j , e_{ij} is the strength of a connection divided by the total weight of the network, and $\delta_{M_i M_j}$ is set to 1 when regions are in the same community and 0 otherwise. '+' and '-' superscripts denote all positive and negative connections, respectively.

For each temporal window, the community assignment for each region was assessed 500 times and a consensus partition was identified using a fine-tuning algorithm from the Brain Connectivity Toolbox (BCT, <http://www.brain-connectivity-toolbox.net/>). This then afforded an estimate of both the time-resolved modularity (Q_T) and cluster assignment (C_{iT}) within each temporal window for each participant in the study. All graph theoretical measures were calculated on weighted and signed connectivity matrices, such that no arbitrary thresholding was required (38).

Based on time-resolved community assignments, we estimated within-module connectivity by calculating the time-resolved module-degree Z-score (W_{iT} ; within module strength) for each region in our analysis (Equation 3) (16).

$$W_{iT} = \frac{\kappa_{iT} - \bar{\kappa}_{s_iT}}{\sigma_{\kappa_{s_iT}}} \quad [3]$$

Equation 3 – Module degree Z-score, W_{iT} , where κ_{iT} is the strength of the connections of region i to other regions in its module s_i at time T , $\bar{\kappa}_{s_iT}$ is the average of κ over all the regions in s_i at time T , and $\sigma_{\kappa_{s_iT}}$ is the standard deviation of κ in s_i at time T .

Time- resolved hub structure

The participation coefficient, B_T , quantifies the extent to which a region connects across all modules (i.e. between-module strength) and has previously been used to characterize hubs within brain networks (e.g. see (39)). The B_T for each region was calculated within each temporal window using Equation 4.

$$B_{iT} = 1 - \sum_{S=1}^{n_M} \left(\frac{\kappa_{iST}}{\kappa_{iT}} \right)^2 \quad [4]$$

Equation 4 - Participation coefficient B_{iT} , where κ_{isT} is the strength of the positive connections of region i to regions in module s at time T , and κ_{iT} is the sum of strengths of all positive connections of region i at time T . The participation coefficient of a region is therefore close to 1 if its connections are uniformly distributed among all the modules and 0 if all of its links are within its own module.

Cartographic profiling

To track fluctuations in cartography over time, we created a novel analysis technique that did not require the labeling of each node into a pre-defined cartographic class (16). For each temporal window, we computed a joint histogram of within- and between-module connectivity measures, which we refer to here as a “cartographic profile”. Code for this analysis is freely available at <https://github.com/macshine/integration/>. To test whether the cartographic profile of the resting brain fluctuated over time between two topological extremes, we performed clustering of temporal windows without the use of cartographic class labels. To do so, we classified the joint histogram of each temporal window (which is naïve to cartographic boundaries) over time using a k-means clustering analysis ($k = 2$). As a result of this analysis, each window was assigned to one of two clusters. K-means was repeated with 500 random restarts (i.e. replicates as implemented in the MATLAB *k-means* function) to mitigate the well known sensitivity of k-means to initial conditions. To ensure that the *a priori* choice of two clusters for the k-means analysis was reflective of the broader patterns in the data across multiple values of k , we re-ran the clustering analysis in the discovery cohort of 92 subjects across a range of k (2-20) and then compared the resultant cluster partitions to the $k = 2$ clusters by calculating the mutual information between the each pair of partitions. The partition identified at each value of k was strongly similar to the pattern identified at $k = 2$ (mean

mutual information = 0.400 ± 0.02). This suggests that our choice of utilizing $k = 2$ to cluster the joint histograms over time was reflective of a relatively “natural” clustering pattern in the data.

To explicitly test whether the resting brain fluctuated more frequently than a stationary null model, we calculated the absolute value of the window-to-window difference in the mean B_T score for each iteration of the VAR null model. We then calculated the 95th percentile of this distribution and used this value to determine whether the resting state data fluctuated more frequently than the null model. In the discovery cohort, $16.1 \pm 1.1\%$ of temporal windows were associated with deviations \geq 95th percentile of the VAR null model (i.e. greater than the predicted 5%), suggesting that the resting state was associated with significant dynamic fluctuations in topology. Importantly, the significant fluctuations along the B_T axis remained after correcting for ongoing changes in the number of modules per temporal window.

To estimate patterns of topology associated with each state, the original 3D connectivity matrix containing MTD values was then reorganized into those windows associated with the two states. The modularity of each window was then calculated using the Louvain algorithm (Equation 2) and the resultant values were then compared statistically using an independent samples t-test (given the higher frequency of the integrated state, a random sub-sample of these windows were selected to match the frequency of the segregated state). Importantly, the two states were matched on graph density. A similar technique was used to estimate the global efficiency of each temporal window. As global efficiency (Equation 5) cannot be computed from networks with negative

weights (20), we first thresholded the connectivity matrix within each window at 5% density and then binarized the resultant matrix before calculating global efficiency.

$$E_{glob} = \frac{2}{n(n-1)} \sum_{i < j \in G} \frac{1}{d(i,j)} \quad [5]$$

Equation 4 – global efficiency of a network, where n denotes the total nodes in the network and $d(i,j)$ denotes the shortest path between a node i and neighboring node j .

To estimate the patterns of brain connectivity associated with each state, we calculated a point-biserial correlation of each region-by-region connectivity measure and the vector representing state identity. Resultant Pearson's correlation coefficients were then normalized using a Fisher's r-to-Z transform and compared between the two states using a paired-samples t-test (FDR, $p < 0.05$). The pairs of regions that survived correction were then reorganized according to a pre-defined network identity vector (35) and projected onto 375 x 375 adjacency matrix (Figure S5).

Task-based alterations in the cartographic profile

To assess task-based functional connectivity, preprocessed data from the original 92 unrelated subjects from the discovery cohort were collected while these subjects performed two different tasks in the fMRI (20): i) a simple motor task in which the participants were presented with visual cues that required them to tap their left or right fingers, squeeze their left or right toes, or move their tongue in 12 second blocks of movement (each movement is repeated twice over the course of the experiment); and ii) a visually-based N-back task, which consisted of interleaved 10 second blocks of a high (2-back) and low (0-back) load N-back

task, each block with object stimuli in one of four classes (places, faces, body parts and tools; see (30) for further details of each experimental paradigm). The mean time series was then extracted from the same 375 regions as defined in the resting state analysis. To control for spurious patterns of connectivity associated with task-evoked activity, we first regressed the HRF-convolved task block data from each time series. The MTD metric was then calculated on the residuals of this regression using a window length of 14 TRs (~10 seconds at 0.72 second TR). These data were then subjected to a cartographic profiling analysis in a similar fashion to the resting state data.

To compare the patterns of time-resolved connectivity across the two tasks to those observed during rest, we tested whether any regions within the 2-dimensional cartographic profile were significantly modulated by task by running a mixed-effects General Linear Model analysis at the individual level, fitting the group-averaged joint histogram to regressors tracking task and rest blocks in both the Motor and the N-back task, separately. We then compared the two tasks and the resting state data statistically using separate two-sided, one-sample t-tests across subjects (FDR $q < 0.05$). Finally, we estimated the relationship between task performance and modularity (Q) and efficiency (E) by calculating each topological measure over time during the task and then correlating the resultant vectors with convolved regressors that represented either task or rest blocks.

In order to assess the alteration in the cartographic profile as a function of task performance, we estimated the affine transformation (using a correlation cost function with 3 degrees of freedom, including translation and rotation parameters) between each individual subjects' resting state cartographic profile

and the profile observed in both the motor and N-back task, separately. The transformation matrices were then entered into a mixed-effects analysis comparing the movement of the cartographic profile as a function of task. Finally, to determine whether the cartographic profile dynamically reorganized as a function of task demands, we correlated the transformed resting state histogram (i.e. the resting state histogram 'shifted' according to the affine transform to match each task profile, as estimated in the previous step) with the histogram for each time point during each task, and the mean correlation for both the task and rest block regressors (trimmed of the first 11 time points in order to control for the trailing BOLD effects of the previous block) for each subject. These values were then averaged (mean) across the cohort of 92 individuals.

To interrogate the relationship between the cartographic profile and behavioral performance, we performed a group-level Pearson's correlation between each bin of the mean joint histogram in each task and two outcome measures associated with the N-back task: the accuracy on the task (percentage of correct responses; Figure 3a) and the mean reaction time on the task (Figure 3b). For each comparison, the null hypothesis of no relationship was rejected after false discovery rate correction ($q < 0.05$).

Replication analysis

To quantify how well our results replicated across sessions and datasets, we calculated group-level correlations between each of the measures identified in our analysis. Overall, we observed a strong positive correlation between the outcome measures identified in the two sessions (for all statistical tests, $p <$

0.001): graph measures – $r_{W_T} = 0.982$, $r_{B_T} = 0.957$ (Figure S6); and mean cartographic profiles $r_{Cart} = 0.982$ (Figure S7). We also confirmed the presence of these results in a unique cohort of 92 unrelated participants from the HCP: graph measures – $r_{W_T} = 0.971$, $r_{B_T} = 0.967$ (Figure S6); and mean cartographic profiles – $r_{Cart} = 0.973$ (Figure S7).

We also observed similarly positive relationships between the group-level outcome measures estimated from the HCP and NKI data (for all statistical tests, $p < 0.001$): graph measures – $r_{W_T} = 0.941$, $r_{B_T} = 0.857$ (Figure S6); and mean cartographic profiles – $r_{Cart} = 0.927$ (Figure S7).

Finally, the linear relationships between behavioral performance and the cartographic profile were consistent across the discovery and replication datasets. Indeed, a spatial correlation between the two datasets was strongly positive for both the relationship with accuracy ($r = 0.613$, $p < 0.001$) and reaction time ($r = 0.681$, $p < 0.001$).

Validation analysis

Based on the novel methodology and short temporal windows utilized in this analysis, we performed numerous additional analyses to clarify the relationship between the main temporal outcome measures calculated in this study with respect to: i) the choice of functional connectivity algorithm; ii) the use of short windows; iii) the choice of high pass filter threshold; iv) the potential adverse effects of spurious noise during the resting state scanning session; and v) the choice of community detection algorithm.

Effect of connectivity algorithm

We have previously shown that the MTD is more sensitive and specific to subtle shifts in connectivity structure than those estimated using a sliding-window Pearson's correlation in simulated BOLD data (14). To determine whether using a sliding-window Pearson's correlation gave similar results to the MTD in this study, we re-analyzed the data in our experiment using a Pearson's correlation with a sliding window of $w = 14$ (the window length used in our experiment) and $w = 83$ (which equates to ~60 seconds, a commonly used window length in the neuroimaging literature) (40). The cartographic profiling results were distinctly different between the two measures. Importantly, the results of the sliding window Pearson's analyses were less reproducible than the MTD across datasets at $w = 14$. This may be due to the different spectral profiles of the two measures, as the MTD preferentially focus on the highest frequency signals in the data (here, after filtering, ~0.1 Hz), whereas Pearson's correlations instead target the slowest frequency signals in the data (here, ~0.017 Hz).

Effect of window length

To determine the effects of using a short window length in the calculation of the MTD on the outcome measures in our experiment, we re-ran the analysis in all 92 subjects from the original group across a range of window lengths (10-100 in intervals of 5 TRs). We then compared the main outcomes measures in our study (parcel-wise mean W_T , mean B_T and the cartographic profile) across all window lengths in all 92 subjects using a region-wise Spearman's rho correlation. There were observable differences between the cartographic profiles when calculated at different window lengths (i.e. longer windows led to less fluctuations and hence, an estimate of the connectome as stationary). Importantly, the frequency of fluctuations (estimated as the frequency of fluctuations along the B_T axis over

time) was greater than expected by a stationary null mode and also reliable at window lengths of 14 TRs (here, approximately 10 seconds), suggesting that the MTD affords a reliable means for tracking spatiotemporal dynamics in fMRI BOLD data.

Effect of high pass filter threshold

Recent work on simulated time series has suggested that low frequency signals in fMRI BOLD data can spuriously effect estimates of sliding window covariance (40), and as such, it has been recommended that the lower bounds of the high pass filter used on BOLD data be set to the reciprocal of the window length used in the sliding window analysis (in our study, this would amount to a low pass filter of $\frac{1}{10.08}$ seconds ~ 0.1 Hz). In contrast, others have shown that using data with a high signal to noise ratio can effectively mitigate the potential issues with aliasing (41). In addition, we have previously shown that the MTD is relatively insensitive to low frequency fluctuations (14), as the temporal differencing used to create the MTD renders the technique relatively insensitive to signals with a lower frequency than the upper bounds of the low pass filter. As such, in keeping with others (11), we chose to use a high pass filter of 0.071 Hz in our study. However, to explicitly test whether the inclusion of low frequency altered the outcome measures in our experiment, we re-ran our analysis over a range of high pass filters (0.001 to 0.1, in steps of 0.1), with a low pass filter of 0.125. Across this entire range, we did not observe any group-level differences in our outcome measures of interest (minimum $r = 0.718$, $p < 0.001$), confirming that the signals measured by the MTD were not adversely affected by spurious low frequency signals in the data.

Effect of preprocessing strategies

To determine whether head motion was associated with each measure, we calculated the first principal component of the 12 head motion parameters over time and then correlated this new vector with each outcome measure. We also correlated the framewise displacement as well as the DVARS values with each outcome measure. None of these correlations was significant at $p < 0.05$. To test for the effects of temporal ‘scrubbing’ (33) and global signal regression, we re-analyzed data for the original group of 92 subjects separately and then compared the outcomes measures across analyses. For the scrubbing analysis, time points associated with framewise displacement $> 0.5\text{mm}$ or DVARS $> 5\%$ were removed and missing data points were then imputed using linear interpolation. Using this technique, we observed strong positive correlations between outcomes measures across analyses (mean Pearson’s $r > 0.700$ for all comparisons), suggesting that neither preprocessing strategy had a major effect on topological or topographic measures calculated using the MTD. Finally, to determine whether physiological sources of noise were associated with each measure, we convolved the heart rate and respiratory signals with a pre-defined transfer function (42) and then correlated the resultant vector either each outcome measure for the 92 subjects from the discovery group. In both instances, we did not observe a significant correlation between the outcomes of interest in our analysis and physiological signals (for each comparison, $r < |0.050|$, $p > 0.05$).

Effect of community detection algorithm

To ensure that the modularity assignment within each window was robust across community detection algorithms, we repeated the analysis using the Infomap algorithm (43) in the discovery cohort and observed broadly consistent results (mean mutual information between community partitions = 0.342 ± 0.16).

Furthermore, we also used another popular method, multi-slice community detection (44), to detect community structure in the time-resolved brain. The temporal modules identified by this method (using standard parameters: $\gamma = \omega = 1$) also gave similar results (mean mutual information between community partitions = 0.447 ± 0.21). However, due to practical concerns regarding computational load and the fact that the Infomap algorithm requires the thresholding of an adjacency matrix (and as such, is insensitive to anti-correlations), we did not use either method for the full study.

Supplementary Figures

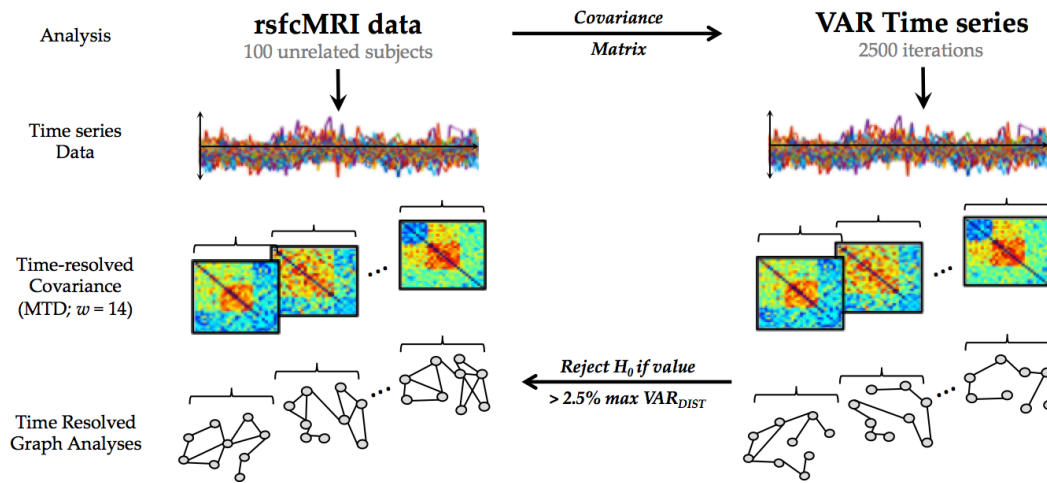


Figure S1: Experimental Design: time series data from 375 brain regions were extracted from 100 unrelated young adults (made available by the Human Connectome Project) and subjected to time-resolved connectivity analysis. After preprocessing, time-resolved functional connectivity was estimated using the Multiplication of Temporal Derivatives, which resulted in a weighted adjacency matrix for each temporal window. Community structure was computed within each temporal window, enabling the calculation of time-resolved module-degree Z-score (W_T) and participation coefficient (B_T). These values were then subjected to cartographic analysis of time-resolved functional connectivity. To test our results against the null model of stationarity, the covariance matrix from the resting state data was used to create 2500 unique null datasets using a Vector Autoregressive Model (denoted with subscript, VAR – i.e. W_{VAR} and B_{VAR}). This data was then subjected to an identical analysis pipeline, with the maximum statistic from each iteration extracted to populate a null distribution, against which results from the resting state data were compared for hypothesis testing.

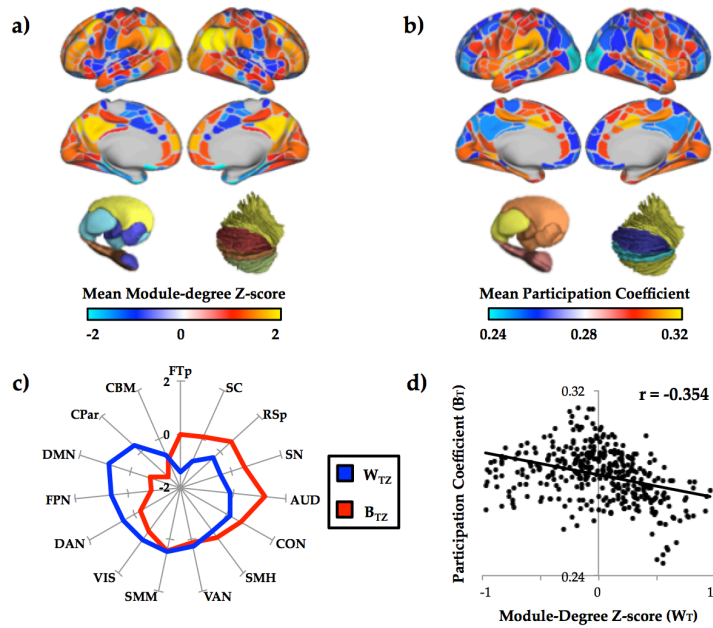


Figure S2: Within- and Between-module connectivity: a) mean within-module connectivity calculated using the module-degree Z-score, W_T , within each temporal window (*Equation 3: Supplementary Materials*); b) between-module connectivity was computed using the participation coefficient, B_T (*Equation 4: Supplementary Materials*); c) individual resting state communities, predefined using the InfoMap community-detection algorithm (43), were differentially balanced towards either high time-resolved intra- (blue) or inter-modular connectivity (red); d) we observed an inverse correlation between mean W_T and mean B_T across all 100 subjects ($r = -0.354$, $p < 0.001$) that was not present in the VAR null data ($r = 0.898$, $p < 0.001$). Key: Aud – Auditory; CON – Cingulo-Opercular; Cpar – Cingulo-parietal; DMN – Default Mode; DAN – Dorsal Attention; FPN – Frontoparietal; FTP – Fronto-temporal; RSp – Retrosplenial; SN – Salience; SMH – Somatomotor Hand; SMM – Somatomotor Mouth; VAN – Ventral Attention; VIS – Visual; SC – Subcortical; CBM – Cerebellum.

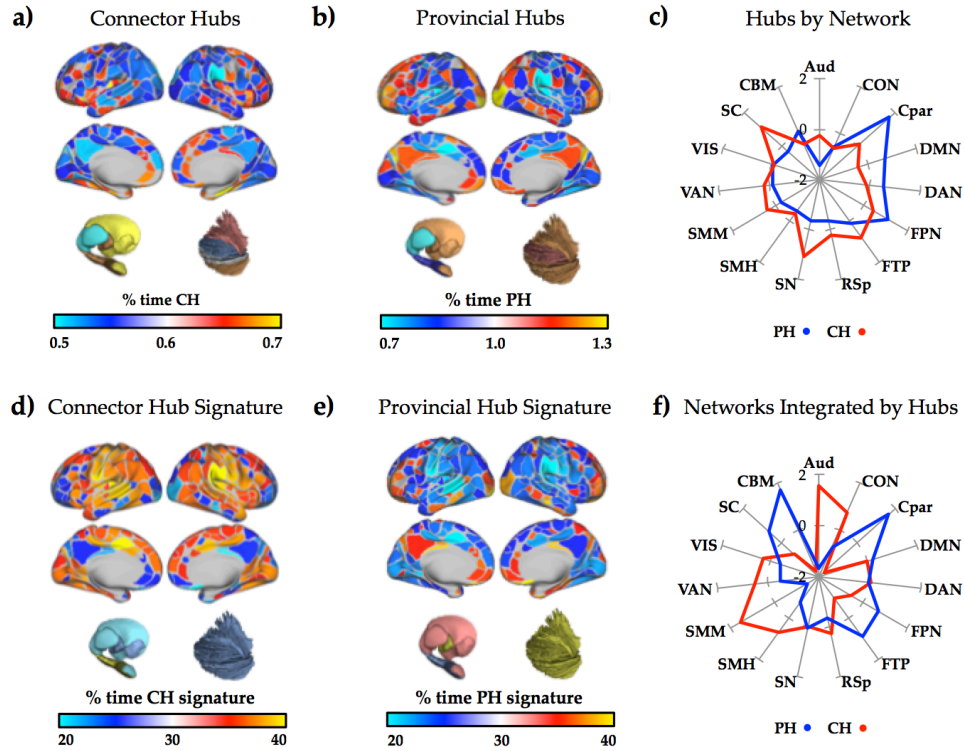


Figure S3: Dynamic Hub Structure in the Resting Brain. a) The regional pattern associated with regions that spent the highest proportion of the resting state session acting as a connector hub (red/yellow), with respect to all other regions; b) regional pattern associated with preferential increase in time acting as a provincial hub (red/yellow), with respect to all other regions; c) Z-scored mean percentage of time acting as either a connector or provincial hub, collapsed into each of 15 pre-defined large-scale cortical networks (16); d) the regional pattern associated with regions that spent the most time within the same module as a connector hub (red/yellow), with respect to all other regions; e) the regional pattern associated with preferential increase in time occurring within the same module as a provincial hub (red/yellow), with respect to all other regions; f) Z-scored mean percentage of time within the same module as a connector or provincial hub, collapsed into each of 15 pre-defined brain systems defined in a previous time-averaged study (4,39). Images available at <http://neurovault.org/collections/HAWDIOCD/>. Key: Aud – Auditory; CON – Cingulo-Opercular; Cpar – Cingulo-parietal; DMN – Default Mode; DAN – Dorsal Attention; FPN – Frontoparietal; FTP – Fronto-temporal; RSp – Retrosplenial; SN – Salience; SMH – Somatomotor Hand; SMM – Somatomotor Mouth; VAN – Ventral Attention; VIS – Visual; SC – Subcortical; CBM – Cerebellum.

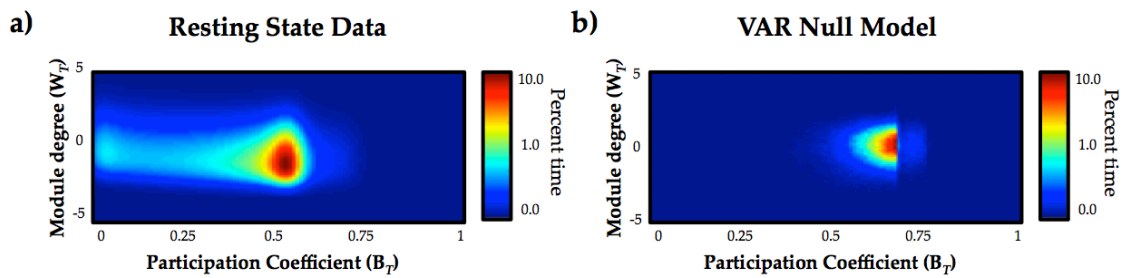


Figure S4: Cartographic profile of resting state and VAR null model: a) mean cartographic profile of resting state across discovery cohort; b) mean cartographic profile of VAR stationary null data.

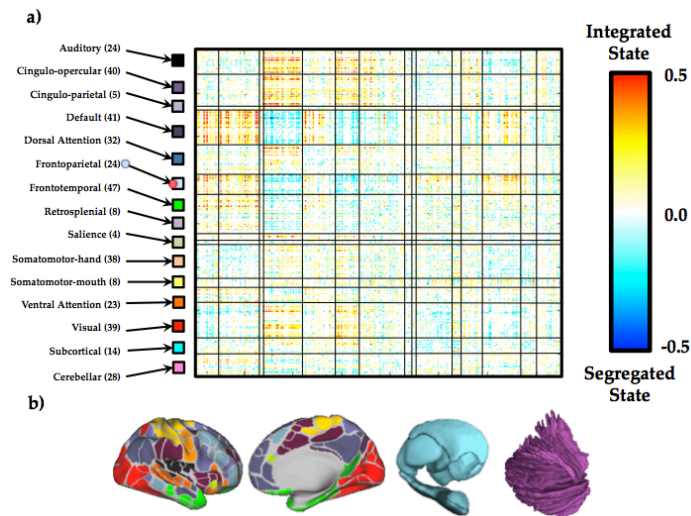


Figure S5: Regional connectivity differences between states: a) Significant differences in the mean connectivity matrix between the two States are plotted in yellow/red (Integrated State) and blue (Segregated State). Only results that survived correction after an independent-samples t-test with FDR 0.05 correction for multiple comparisons are shown; b) rows and columns reflect each of the 375 brain regions, organized according to clustering approach outlined in Gordon et al., 2014.

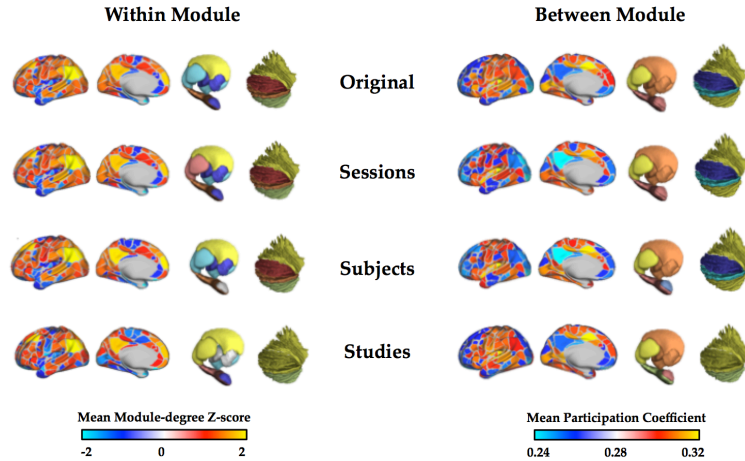


Figure S6: Replication of Within- and Between-module connectivity scores: spatial projection of W_T and B_T scores for the left hemisphere, subcortical and cerebellar regions for all subjects from each of the four samples used in the study. Original – discovery cohort; Sessions – comparison across resting state sessions in the discovery cohort; Subjects – comparison across a unique group of unrelated subjects; Studies – comparison across studies (NKI Rockland dataset).

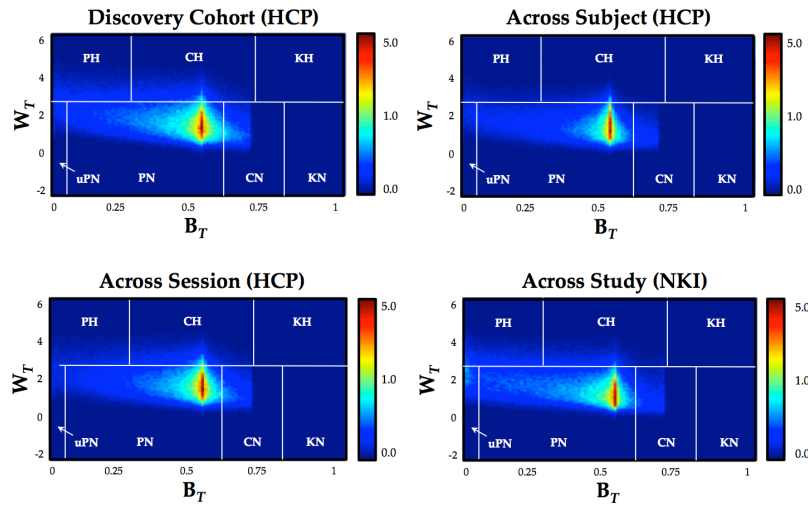


Figure S7: Replication of Cartographic Profiles: mean joint histograms for single subject from each of the four samples using in the study, comparing the distribution of W_T and B_T values over each temporal window.

Figure S8: Temporal fluctuations in integration and segregation in the resting state: movie of a cartographic profile of resting state data from a single subject from the HCP dataset (subject #100307).

Figure S9: Temporal fluctuations in integration and segregation in the resting state: movie of a cartographic profile of resting state data from a single subject from the NKI Rockland dataset (subject #0102157).

Figure S10: Temporal fluctuations in integration and segregation during task performance: movie of a cartographic profile of N-back data from a single subject from the HCP dataset (subject #100307). A bar chart detailing the current block of the experiment is projected next to the cartographic profile.

Acknowledgements

The data reported in this paper were made publicly available by the Human Connectome Project and 1000 Functional Connectomes project. There were no conflicts of interest for any authors. JMS, OK, PTB and RAP designed the analysis. JMS performed the analysis and wrote the first draft. JMS, PTB, OK, PGB, KJG, CAM and RAP reviewed and edited the manuscript. We would like to thank Vanessa Sochat for her assistance with the implementation of the analysis, Michael Riis and Ian Eisenberg for their helpful insights and Tim Laumann, Claire O'Callaghan, and Rav Suri for their critical review of the manuscript.

References

1. Petersen SE, Sporns O. Brain Networks and Cognitive Architectures. *Neuron*. 2015 Oct 7;88(1):207–19.
2. Dehaene S, Changeux JP, Naccache L. Conscious, preconscious, and subliminal processing: a testable taxonomy. *Trends in Cognitive Sciences*. 2006;10(5):204–11.
3. Tononi G, Sporns O. A measure for brain complexity: relating functional segregation and integration in the nervous system. *Proceedings of the ...* 1994;91:5033–7.
4. van den Heuvel MP, Sporns O. Network hubs in the human brain. *Trends in Cognitive Sciences*. 2013 Dec;17(12):683–96.
5. Sporns O. Network attributes for segregation and integration in the human brain. *Current Opinion in Neurobiology*. 2013 Apr;23(2):162–71.
6. Varela F, Lachaux JP, Rodriguez E. The brainweb: phase synchronization and large-scale integration. *Nature reviews ...* 2001;2:229–39.
7. Deco G, Tononi G, Boly M, Kringelbach ML. Rethinking segregation and integration: contributions of whole-brain modelling. *Nat Rev Neurosci*. Nature Publishing Group; 2015 Jul;16(7):430–9.
8. Shen K, Hutchison RM, Bezgin G, Everling S, McIntosh AR. Network structure shapes spontaneous functional connectivity dynamics. *J Neurosci*. Society for Neuroscience; 2015 Apr 8;35(14):5579–88.
9. Betzel RF, Fukushima M, He Y, Zuo X-N, Sporns O. Dynamic fluctuations coincide with periods of high and low modularity in resting-state functional brain networks. *NeuroImage*. 2015 Dec 11;127:287–97.
10. Cole MW, Bassett DS, Power JD, Braver TS, Petersen SE. Intrinsic and task-evoked network architectures of the human brain. *Neuron*. 2014 Jul 2;83(1):238–51.
11. Bassett DS, Yang M, Wymbs NF, Grafton ST. Learning-induced autonomy of sensorimotor systems. *Nat Neurosci*. 2015 May;18(5):744–51.
12. Barttfeld P, Uhrig L, Sitt JD, Sigman M, Jarraya B, Dehaene S. Signature of consciousness in the dynamics of resting-state brain activity. *Proc Natl*

- Acad Sci USA. National Acad Sciences; 2015 Jan 20;112(3):887–92.
13. Zalesky A, Fornito A, Cocchi L, Gollo LL, Breakspear M. Time-resolved resting-state brain networks. *Proceedings of the National Academy of Sciences*. 2014 Jul 15;111(28):10341–6.
 14. Shine JM, Koyejo O, Bell PT, Gorgolewski KJ, Gilat M, Poldrack RA. Estimation of dynamic functional connectivity using Multiplication of Temporal Derivatives. *NeuroImage*. 2015;122:399–407.
 15. Smith SM, Beckmann CF, Andersson J, Auerbach EJ, Bijsterbosch J, Douaud G, et al. Resting-state fMRI in the Human Connectome Project. *NeuroImage*. 2013 Oct 15;80:144–68.
 16. Guimerà R, Nunes Amaral LA. Functional cartography of complex metabolic networks. *Nature*. 2005 Feb 24;433(7028):895–900.
 17. Sporns O. Cerebral cartography and connectomics. *Philos Trans R Soc Lond, B, Biol Sci*. 2015 May 19;370(1668):20140173–3.
 18. Sporns O, Betzel RF. Modular Brain Networks. *Annu Rev Psychol*. Annual Reviews 4139 El Camino Way, PO Box 10139, Palo Alto, California 94303-0139, USA; 2015 Sep 21;67(1):annurev-psych-122414-033634.
 19. Mattar MG, Cole MW, Thompson-Schill SL, Bassett DS. A Functional Cartography of Cognitive Systems. Honey CJ, editor. *PLoS Comput Biol*. Public Library of Science; 2015 Dec;11(12):e1004533.
 20. Barch DM, Burgess GC, Harms MP, Petersen SE, Schlaggar BL, Corbetta M, et al. Function in the human connectome: task-fMRI and individual differences in behavior. *NeuroImage*. 2013 Oct 15;80:169–89.
 21. Mišić B, Sporns O, McIntosh AR. Communication efficiency and congestion of signal traffic in large-scale brain networks. Bassett DS, editor. *PLoS Comput Biol*. Public Library of Science; 2014 Jan;10(1):e1003427.
 22. Krienen FM, Yeo BTT, Buckner RL. Reconfigurable task-dependent functional coupling modes cluster around a core functional architecture. *Philos Trans R Soc Lond, B, Biol Sci*. 2014 Oct 5;369(1653):20130526–6.
 23. Cole MW, Reynolds JR, Power JD, Repovs G, Anticevic A, Braver TS. Multi-task connectivity reveals flexible hubs for adaptive task control. *Nat*

- Neurosci. Nature Publishing Group; 2013 Sep 1;16(9):1348–55.
24. Berman MG, Mišić B, Buschkuhl M, Kross E, Deldin PJ, Peltier S, et al. Does resting-state connectivity reflect depressive rumination? A tale of two analyses. *NeuroImage*. 2014 Dec;103:267–79.
 25. Kitzbichler MG, Henson RNA, Smith ML, Nathan PJ, Bullmore ET. Cognitive effort drives workspace configuration of human brain functional networks. *J Neurosci*. 2011 Jun 1;31(22):8259–70.
 26. Tononi G, Edelman GM. Consciousness and complexity. *Science*. 1998;282(5395):1846–51.
 27. Edelman GM. Naturalizing consciousness: a theoretical framework. *Proceedings of the National Academy of ...*. 2003;100(9):5520–4.
 28. van den Heuvel MP, Sporns O. An anatomical substrate for integration among functional networks in human cortex. *J Neurosci*. 2013 Sep 4;33(36):14489–500.
 29. Honey CJ, Thesen T, Donner TH, Silbert LJ, Carlson CE, Devinsky O, et al. Slow cortical dynamics and the accumulation of information over long timescales. *Neuron*. 2012 Oct 18;76(2):423–34.
 30. Glasser MF, Sotiropoulos SN, Wilson JA, Coalson TS, Fischl B, Andersson JL, et al. The minimal preprocessing pipelines for the Human Connectome Project. *NeuroImage*. 2013 Oct;80:105–24.
 31. Nooner KB, Colcombe SJ, Tobe RH, Mennes M, Benedict MM, Moreno AL, et al. The NKI-Rockland Sample: A Model for Accelerating the Pace of Discovery Science in Psychiatry. *Front Neurosci*. Frontiers Media SA; 2012;6:152.
 32. Avants BB, Epstein CL, Grossman M, Gee JC. Symmetric diffeomorphic image registration with cross-correlation: evaluating automated labeling of elderly and neurodegenerative brain. *Med Image Anal*. 2008 Feb;12(1):26–41.
 33. Power JD, Mitra A, Laumann TO, Snyder AZ. Methods to detect, characterize, and remove motion artifact in resting state fMRI. *NeuroImage*. 2014.

34. Behzadi Y, Restom K, Liao J, Liu TT. A component based noise correction method (CompCor) for BOLD and perfusion based fMRI. *NeuroImage*. 2007 Aug;37(1):90–101.
35. Gordon EM, Laumann TO, Adeyemo B, Huckins JF, Kelley WM, Petersen SE. Generation and Evaluation of a Cortical Area Parcellation from Resting-State Correlations. *Cereb Cortex*. Oxford University Press; 2014 Oct 14;:bhu239.
36. Diedrichsen J, Balsters JH, Flavell J, Cussans E, Ramnani N. A probabilistic MR atlas of the human cerebellum. *NeuroImage*. 2009 May 15;46(1):39–46.
37. Nichols TE, Holmes AP. Nonparametric permutation tests for functional neuroimaging: a primer with examples. *Hum Brain Mapp*. 2002 Jan;15(1):1–25.
38. Rubinov M, Sporns O. Complex network measures of brain connectivity: Uses and interpretations. *NeuroImage*. 2010 Sep;52(3):1059–69.
39. Power JD, Schlaggar BL, Lessov-Schlaggar CN, Petersen SE. Evidence for hubs in human functional brain networks. *Neuron*. 2013 Aug 21;79(4):798–813.
40. Leonardi N, Van De Ville D. On spurious and real fluctuations of dynamic functional connectivity during rest. *NeuroImage*. 2015 Jan 1;104:430–6.
41. Zalesky A, Breakspear M. Towards a statistical test for functional connectivity dynamics. *NeuroImage*. 2015 Jul 1;114:466–70.
42. Chang C, Glover GH. Time-frequency dynamics of resting-state brain connectivity measured with fMRI. *NeuroImage*. 2010 Mar;50(1):81–98.
43. Rosvall M, Bergstrom CT. Maps of random walks on complex networks reveal community structure. *Proc Natl Acad Sci USA*. 2008 Jan 29;105(4):1118–23.
44. Mucha PJ, Richardson T, Macon K, Porter MA, Onnela J-P. Community structure in time-dependent, multiscale, and multiplex networks. *Science*. American Association for the Advancement of Science; 2010 May 14;328(5980):876–8.